INSTITUTE OF PHYSICS PUBLISHING JOURNAL OF PHYSICS G: NUCLEAR AND PARTICLE PHYSICS

J. Phys. G: Nucl. Part. Phys. **29** (2003) 2763–2775 PII: S0954-3899(03)68927-9

Planar and aplanar tilted bands in the odd–odd nucleus ^{132}Cs

G Rainovski[1,8], E S Paul[1], H J Chantler[1], P J Nolan[1], D G Jenkins[2], R Wadsworth[2], P Raddon[2], A Simons[2], D B Fossan[3], T Koike[3], K Starosta[3], C Vaman[3], E Farnea[4], A Gadea[4], Th Kröll[4], G de Angelis[4], R Isocrate[5], D Curien[6] and V I Dimitrov[7]

[1] Oliver Lodge Laboratory, University of Liverpool, Liverpool L69 7ZE, UK
[2] Department of Physics, University of York, Heslington, York Y01 5DD, UK
[3] Department of Physics and Astronomy, SUNY at Stony Brook, Stony Brook, NY 11794-3800, USA
[4] INFN, Laboratory Nazioanly di Legnaro, Legnaro I-35020, Italy
[5] INFN, Sezione di Padova, Padova I-35131, Italy
[6] Institut de Recherches Subatomiques, Strasbourg, F67037, France
[7] University of Notre Dame, Notre Dame, IN 46556, USA

E-mail: rig@ns.ph.liv.ac.uk

Received 27 August 2003
Published 12 November 2003
Online at stacks.iop.org/JPhysG/29/2763

Abstract

High-spin states in the doubly odd $N = 77$ nucleus ^{132}Cs have been studied. Gamma-ray linear polarization and angular correlation measurements have been performed to determine the spin and parity of the states. A rotational sequence of enhanced dipole transitions was established. This band can be described within the framework of the the tilted axis cranking (TAC) model as a band based on a weakly deformed structure in which the total angular momentum vector does not coincide with any of the principal axes of the triaxial nucleus but still is in the plane defined by the short and long axes. The theoretical description of the previously proposed chiral bands in ^{132}Cs was extended in the framework of the core–particle coupling model (CPCM) confirming that the total angular momentum for the $\pi h_{11/2} \otimes \nu h_{11/2}$ configuration is well outside any planes defined by the principal axes of the nucleus and revealing the important role of the residual proton–neutron interaction between the valence particles.

1. Introduction

Many properties of nuclear rotation can be easily understood as consequences of certain symmetries [1]. Among them chiral rotation of triaxial nuclei and magnetic rotation in weakly

[8] On leave from Faculty of Physics, St. Kliment Ohridski University of Sofia, 1164 Sofia, Bulgaria.

deformed nuclei are two phenomena which have attracted significant interest during the last decade.

The concept of magnetic rotation was introduced at the beginning of the 1990s [2] in order to explain experimentally observed regular $\Delta I = 1$ bands in some weakly deformed, near spherical lead nuclei [3]. Nowadays, it is understood as a consequence of symmetry breaking [4]. A simplified description of magnetic rotation can be given as follows: currents of a small number of valence high-j particles and high-j holes tend to be oriented perpendicularly to each other in a weakly deformed (nearly spherical) nucleus. As a result, their angular momenta $\vec{j}_\pi$ and $\vec{j}_\nu$ couple to a total angular momentum vector $\vec{I}$, which is tilted with respect to the principal axes of the nucleus. This coupling causes breaking of the signature symmetry with respect to the intrinsic frame which leads to the appearance of $\Delta I = 1$ sequences in the laboratory frame [4]. The total angular momentum is increased by the gradual alignment of $\vec{j}_\pi$ and $\vec{j}_\nu$ along the rotational axis, a process which is named the 'shears' mechanism. The magnetic moment has a large transverse component, $\mu_\perp$, which gives rise to the enhanced $M1$ transition strength in the shears band. The magnetic dipole bands are described within the framework of the tilted axis cranking (TAC) model [2].

Chirality is a recently proposed symmetry of nuclear rotations [4]. A spontaneous breaking of this symmetry can take place for configurations where the angular momenta of the valence protons, the valence neutrons and the core are mutually perpendicular. This can occur when the Fermi level is located in the lower part of a valence proton high-j (particle-like) subshell and in the upper part of a valence neutron high-j (hole-like) subshell, and the core is essentially triaxial. The angular momenta of the valence particles are then aligned along the short and long axes of the triaxial core, while the angular momentum of the rotational core is aligned along the intermediate axis. These three mutually perpendicular angular momenta divide the space in the body-fixed frame into eight octants. The total angular momentum $\vec{I}$, which is tilted with respect to the planes defined by the principal axes of the nucleus, introduces chirality by selecting one of the octants. In four octants the angular momenta of the core and the valence particle form a left-hand system, and in the other four a right-hand system [4]. Since the chiral and the signature symmetries are broken in the body-fixed system their restoration in the laboratory frame generates doublet $\Delta I = 1$ bands which nearly energetically degenerate in a certain spin region.

The TAC model predicts several mass regions of the nuclear chart where magnetic bands can appear [1, 2]. The predictions are consistent with experimentally observed magnetic dipole bands as summarized in [5]. Among these mass regions there is also a wide region around $50 < Z < 64$ and $76 < N < 82$. In this region the particle-like protons fill successively the $d_{5/2}$ and $g_{7/2}$ subshells and the high-j $h_{11/2}$ intruder, while the neutrons in the high-j $h_{11/2}$ intruder are hole-like. So far several $\Delta I = 1$ bands have been established around the border of this region [5]. However, there is a spot around $50 < Z < 57$ and $76 < N < 82$, where the magnetic dipole bands still have not been observed. Partially, this is due to the fact that the nuclei with $50 < Z < 57$ and $76 < N < 82$ are experimentally difficult to access in heavy-ion fusion reactions. Chiral twin bands have been proposed in several $N = 73$ [6] and $N = 75$ [7–9] isotones, revealing a small island of chiral rotation centred around ^{134}Pr. All these bands are built on the $\pi h_{11/2} \otimes \nu h_{11/2}$ configuration. A near energy degeneracy is only observed for high-spin states of the twin bands in ^{134}Pr [7]. The chiral partners in other twin bands keep their energy separation at a few hundred keV into the high-spin regime. This energy difference has been understood as a consequence of a weaker violation of chiral symmetry, the so-called chiral vibration [10–12].

The $N = 77$ Cs and La isotopes are situated at the intersection of the island of chirality and the region where magnetic dipole bands are predicted to appear in the mass $A \approx 130$

region [1, 2]. Candidate chiral bands are observed in ^{134}La [13] and ^{132}Cs [14, 15]. In contrast to other nuclei peripheral to ^{134}Pr, the chiral bands in ^{134}La and ^{132}Cs almost reach degeneracy at spin 14^+ but the side bands are not well developed. In our recent study [15], the surprising result that chiral bands still exist in the moderately deformed triaxial nucleus ^{132}Cs has been explained as due to the proton–neutron interaction between the valence particles which produces a perpendicular coupling between their angular momenta. A similar effective interaction is thought to be responsible for the shears mechanism [16]. In this respect ^{132}Cs is an interesting case where the phenomena of magnetic dipole bands and chiral twin bands can coexist, a situation which could prove their common origin. In the present paper we report on new detailed experimental information for ^{132}Cs which confirms the existence of a magnetic dipole band and we conclude our study of the chiral twin bands in this nucleus.

2. Experimental details and results

Excited states in ^{132}Cs were populated in the ^{124}Sn (^{13}C,4n1p) reaction at a beam energy of 75 MeV, as detailed in [15]. The EUROBALL IV γ-ray spectrometer [17] was used in conjunction with the EUCLIDES charged particle ball [18]. A total of 2×10^9 events of mean γ-ray fold 3.8 were collected of which approximately 1% were associated with the emission of one proton. The γ-rays in coincidence with one proton emission were sorted into an $E_\gamma - E_\gamma - E_\gamma$ cube and analysed with the RADWARE [19] programs. Sample coincidence γ-ray spectra are shown in figure 1.

To deduce the multipole order of γ-rays, angular-intensity ratios, based on the directional correlation formalism [20], were analysed. For this purpose proton-gated γ–γ coincidences between detectors placed at backward angles ($\Theta_{\rm av} = 156^\circ$) and detectors placed close to 90° ($\Theta_{\rm av} = 90^\circ$) were sorted into an E_γ–E_γ matrix. Coincidence intensities of transitions were extracted from this matrix and used to calculate ratios $R = I_\gamma\big(\Theta_{\rm av}^{\rm gate} = 90^\circ, \Theta_{\rm av}^{\rm spectrum} = 156^\circ\big)\big/ I_\gamma\big(\Theta_{\rm av}^{\rm gate} = 156^\circ, \Theta_{\rm av}^{\rm spectrum} = 90^\circ\big)$. An angular intensity ratio of 1.0 is expected if the gating and observed transitions are pure stretched transitions with the same multipole order. For the present detector geometry, a value of 0.54 is expected for a pure dipole transition gated on a stretched quadrupole transition. A value of 1.85 is expected for a $\Delta I = 2$ transition using a gate on a $\Delta I = 1$ transition. The linear polarization of the γ-rays was measured by considering the 24 clover detectors as Compton polarimeters [21]. Two γ–γ matrices were sorted with one axis corresponding to a single-hit in any detector in EUROBALL and the second axis corresponding to double-hit scattered clover event. One matrix contains events scattered parallel to the reaction plane, while the other contains the perpendicular scattered events. The experimental linear polarization is defined as $P = (1/Q)(N_\perp - N_\parallel)/(N_\perp + N_\parallel)$, where $N_\perp$ ($N_\parallel$) are the number of added-back photopeak counts scattered in the perpendicular (parallel) reaction plane and Q is the polarization sensitivity of the clover detectors [21]. Positive linear-polarization values correspond to stretched electric transitions, while negative values correspond to stretched magnetic transitions. The results from these measurements are listed in table 1.

The level scheme of ^{132}Cs deduced from the present experiment is shown in figure 2. In the first in-beam study of ^{132}Cs, Hayakawa *et al* [22] identified five structures and three of them, built on the lowest (7^-), (8^-) and the (9^+) states were associated with two quasiparticle excitations involving the $\pi h_{11/2}$ orbital coupled to $\nu d_{5/2}$, $\nu g_{7/2}$ and $\nu h_{11/2}$ orbitals, respectively. Liu *et al* [23] later suggested from smooth systematic trends of energy levels in Cs nuclei that the $\pi h_{11/2} \otimes \nu h_{11/2}$ band is built on the 1131 keV $I^\pi = 9^+$ state. In the present study we have assumed that the spin-parity of the 1131 keV state is reliably determined, but we have to point

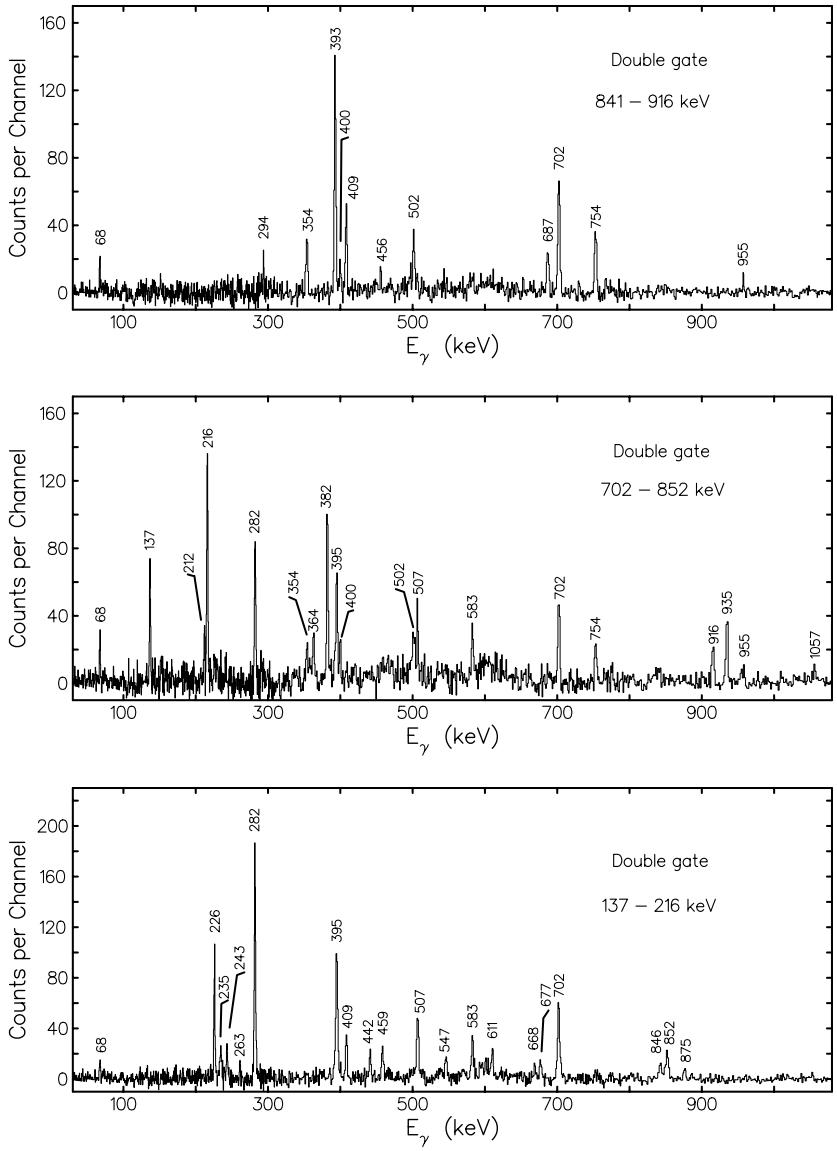

Figure 1. Examples of doubly gated γ-ray coincidence spectra showing the transitions between negative parity states. Peaks labelled with their energy in keV are assigned to ^{132}Cs. Sample spectra showing the transitions between positive parity states can be found in [15].

out that a direct measurement is still missing. The experimental results for positive parity structures in ^{132}Cs from the present study have been reported recently [15]. Here, we would like to stress that we have considerably extended the previously proposed bands 1 and 2 [22]. Additionally, we have observed a new band—band 3. The results from linear polarization and angular correlation measurements (cf table 1) showed that this band was built on the $\pi h_{11/2} \otimes \nu h_{11/2}$ configuration and could be considered as a chiral partner of band 2 [15].

The 1131 keV state is connected by the 594 keV and 344 keV transitions to the 788 keV and 538 keV states, respectively. Both transitions have positive linear polarization values and angular correlation ratios consistent with $\Delta I = 1$ transitions (see table 1). These results

Table 1. Measured properties of the γ-ray transitions assigned to ^{132}Cs.

			R_{dco}			
E_γ (keV)	T_γ [a]	Band	Q[b]	D[c]	Linear polarization	Mult.
67.6(3)	75.2(20)	6 → 4				$(M1/E2)$
136.7(4)	13.7(7)	5	0.58(5)		–0.44(19)	$M1/E2$
146.8(3)	13.8(8)					$M1/E2$
150.5(3)	79.3(25)	2	0.63(5)			$M1/E2$
152.7(4)	25.0(6)					$M1/E2$
162.0(6)	1.7(3)	3		0.91(14)		$M1/E2$
167.2(3)	5.2(5)			1.10(18)		$M1/E2$
212.4(4)	3.2(6)	7				$(M1/E2)$
215.9(3)	31.0(7)	5	0.48(4)		–0.33(20)	$M1/E2$
225.9(3)	100.0(6)	4	0.53(4)		–0.35(10)	$M1/E2$
234.7(4)	2.8(4)	4				$M1/E2$
243.3(4)	2.6(4)	6 → 5				
263.3(6)	2.1(5)	4				$M1/E2$
281.9(3)	21.4(5)	5	0.44(4)		–0.39(21)	$M1/E2$
293.7(4)	2.2(4)	6				$M1/E2$
298.5(4)	7.9(9)	2		1.05(6)	–0.43(16)	$M1/E2$
304.4(4)	10.1(6)	1→ 2	0.46(9)		–0.32(24)	$M1/E2$
310.3(4)	7.0(6)	3		0.96(14)	–0.40(25)	$M1/E2$
313.8(5)	2.9(5)	3		0.83(20)		$M1/E2$
343.6(3)	19.2(9)	2 → 6	0.61(7)		0.61(33)	$E1$
353.8(5)	2.6(5)	7 → 6	0.51(9)			$M1/E2$
360.6(2)	3.0(5)	1				$M1/E2$
363.5(6)	2.2(4)	6	0.66(14)		–0.34(21)	$M1/E2$
378.2(4)	2.5(6)	3		0.86(26)		$M1/E2$
382.1(4)	5.0(6)	6	0.53(5)			$M1/E2$
386.7(4)	8.5(8)		0.48(9)			$M1/E2$
393.1(4)	15.3(8)	6	0.46(6)		–0.56(14)	$M1/E2$
395.1(3)	21.1(6)	5	0.44(7)		–0.48(24)	$M1/E2$
399.7(5)	3.8(6)	7	0.48(7)			$M1/E2$
401.6(3)	27.0(7)	2	0.54(9)		–0.61(12)	$M1/E2$
407.8(3)	40.0(8)	1		1.70(9)	0.64(24)	$E2$
408.5(3)	42.6(9)	6	0.62(6)		–0.53(17)	$M1/E2$
413.7(4)	11.7(6)	1 → 2	0.94(9)	1.59(17)	0.65(42)	$E2$
422.1(3)	8.0(3)					$M1/E2$
424.0(4)	1.7(3)	2				$M1/E2$
428.0(3)	15.4(8)	2	0.62(9)		–0.32(16)	$M1/E2$
442.4(3)	5.5(4)	4				$M1/E2$
445.5(4)	10.7(5)	2	0.50(7)		–0.88(34)	$M1/E2$
447.3(1)	2.1(4)	3 → 2		1.8(5)[d]		$M1/E2$
452.9(5)	4.3(8)	2	0.57(9)		–0.42(15)	$M1/E2$
455.1(5)	3.4(7)	2	0.68(17)		–0.41(28)	$M1/E2$
456.3(3)	0.9(3)	7				$(M1/E2)$
459.3(5)	3.5(6)	6				$M1/E2$
478.0(4)	2.1(4)	2	0.48(10)			$M1/E2$
483.6(3)	3.4(7)	3 → 2	0.69(15)		–0.26(21)	$M1/E2$
494.1(3)	14.4(6)	2 → 6	0.58(8)		0.26(15)	$E1$
496.4(2)	8.9(9)			1.02(9)	–0.26(18)	$M1/E2$

Table 1. (Continued.)

E_γ (keV)	T_γ [a]	Band	R_{dco} Q[b]	R_{dco} D[c]	Linear polarization	Mult.
501.8(2)	1.5(3)	7	0.53(10)			$M1/E2$
507.1(2)	12.7(2)	5	0.47(5)		–0.40(15)	$M1/E2$
518.0(4)	4.3(8)	3→ 2		1.20(21)	–0.36(22)	$M1/E2$
541.0(3)	4.0(9)		0.52(15)			$M1/E2$
546.6(4)	4.5(8)	5 → 4	0.68(10)		–0.23(17)	$M1/E2$
552.5(2)	0.8(4)	6				$M1/E2$
553.3(4)	16.2(8)			1.04(7)	–0.51(23)	$M1/E2$
583.1(4)	9.8(10)	5	0.43(14)		–0.34(17)	$M1/E2$
593.8(2)	85.0(20)	2	0.59(4)		0.24(9)	$E1$
609.3(4)	5.2(9)	3 → 2		0.96(9)	–0.35(19)	$M1/E2$
611.3(3)	6.3(5)	4	0.59(6)		–0.34(28)	$M1/E2$
633.3(4)	19.2(8)	1	0.53(9)			$M1/E2$
667.7(3)	3.8(7)	5				$(M1/E2)$
668.3(3)	5.7(6)	4	1.12(9)			$E2$
677.1(4)	7.4(9)	4		1.51(17)		$E2$
686.8(3)	5.7(8)	6	0.95(11)			$E2$
700.1(4)	27.1(7)	2	0.99(8)		0.60(31)	$E2$
702.1(3)	3.6(7)	5 → 6				$(M1/E2)$
702.2(2)	25.7(7)	6	0.97(5)		0.29(14)	$E2$
703.8(2)	22.7(6)		1.23(15)		0.59(27)	$E2$
706.0(4)	15.7(9)	1 → 2	1.11(20)		0.55(27)	$E2$
726.5(4)	4.7(8)	2		1.7(3)		$E2$
730.2(3)	9.8(11)	1				$(E2)$
753.6(3)	5.3(4)	7 → 6	1.03(10)		0.36(27)	$E2$
759.8(5)	1.0(3)	3 → 2				$(E2)$
826.1(4)	5.6(7)	1	0.79(11)			
832.1(3)	4.8(6)	2	1.2(2)			$E2$
841.5(2)	11.3(6)	6	1.00(9)		0.29(16)	$E2$
846.1(4)	6.6(6)	4	1.05(11)		0.63(22)	$E2$
852.4(3)	10.9(6)	6	0.97(10)		0.47(25)	$E2$
874.6(4)	5.0(6)	4	1.04(20)		0.72(53)	$E2$
876.9(4)	2.0(6)	2	1.31(26)			$E2$
883.1(3)	9.9(8)	2	0.92(9)		0.51(26)	$E2$
900.6(4)	8.2(9)	2	1.02(7)		0.66(33)	$E2$
916.0(3)	9.7(8)	6	0.95(9)			$E2$
923.6(4)	4.1(7)	2	1.10(10)		0.65(38)	$E2$
930.9(4)	7.3(6)	2	1.22(13)		0.53(13)	$E2$
934.6(5)	4.4(9)	6	1.02(9)			$E2$
955.0(5)	0.9(3)	6				$(E2)$
993.8(3)	26.2(7)	1	0.91(17)		0.65(24)	$E2$
996.8(3)	14.4(6)	1	1.27(21)		0.40(22)	$E2$
1057.4(4)	5.2(9)	7 → 6	1.19(16)		0.38(29)	$E2$
1310.2(3)	4.2(8)	1	1.06(14)			$E2$

[a] Relative γ-ray intensity normalized to 100% for the 225.9 keV transition ($8^- \rightarrow 7^-$).
[b] Angular intensity ratios obtained by gating on stretched quadrupole transitions.
[c] Angular intensity ratios obtained by gating on stretched dipole transitions.
[d] Angular intensity ratios for non-stretched $\Delta I = 1$ transitions are the same as for $\Delta I = 2$ transitions.

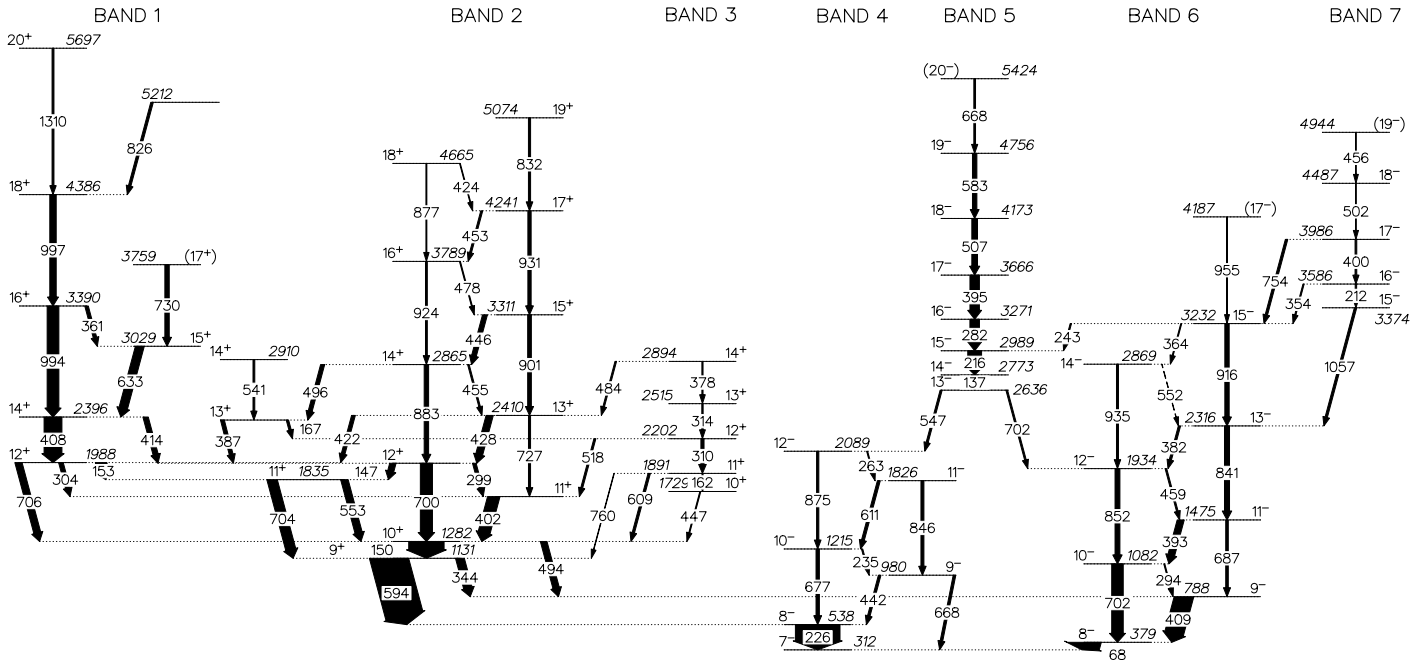

Figure 2. Level scheme of ^{132}Cs deduced from the present work. The energies of the γ transitions and of the levels are given in keV. The thickness of the arrows are proportional to the γ-ray intensities.

strongly suggest a change in parity and confirm the tentatively proposed spin-parities 8^- and 9^- [22] for the 538 keV and 788 keV states, respectively. The 226 keV transition which links the 538 keV state with the 312 keV state has a linear polarization value and an angular correlation ratio consistent with a $M1/E2$ transition. This provides 7^- for the spin-parity of the 312 keV state. We have not observed any transition below the 312 keV state which suggests that this state is isomeric. Such an isomeric state can be expected since Hayakawa *et al* [22] have proposed that the 312 keV state decays by a 72 keV $E2$ transition which should be strongly hindered.

Bands 4 and 6 are built on 7^- and 8^- states, respectively. The present study confirms the level structure for these bands proposed by Hayakawa *et al* [22] and provides detailed spectroscopic information about the multipolarities of the γ-ray transitions (see table 1). We were not able to observe the tentatively proposed 1076 keV transition at the top of band 4. This band becomes strongly non-yrast above spin 12 and most of the γ-ray intensity below spin 12 comes from the decay of band 5 (see figure 2). We have observed a new transition of energy 955 keV on the top of band 6. At spin 15, band 6 crosses with another new structure—band 7. This is a irregular structure which decays to band 6 by 1057 keV, 754 keV and 354 keV transitions. The linear polarization values and angular correlation ratios for the 1057 keV and 754 keV transitions show that these are $E2$ transitions providing spin-parity 17^- and 15^- for the 3986 keV and 3374 keV states. The angular correlation ratios for the 400 keV, 354 keV and 502 keV transitions are consistent with $\Delta I = 1$ spin change, suggesting 16 and 18 for the spins of the 3586 keV and 4487 keV levels, respectively. Since a change of parity within this structure is unlikely we have assumed that band 7 consists of $M1/E2$ transitions.

Band 5 has been observed in [22]. In the present study we have extended this band up to spin 20 and firmly connected it to bands 4 and 6. However, we were not able to confirm the tentatively proposed 785 keV transition [22] which is supposed to connect the 2773 keV state of band 5 with the 12^+ 1988 keV state. In fact, we were not able to observe any transitions connecting band 5 to the positive parity levels. The angular correlation ratio for the 547 keV γ-ray suggests spin 13 for the 2636 keV level—one unit more than the tentatively proposed spin in [22]. The measured linear polarization for the 547 keV transition is consistent with a magnetic transition (see table 1) confirming that band 5 has negative parity. The 137 keV transition which decays from the 2773 keV 14^- level is about three times less intense than the 216 keV transition which populates the same level. Such a difference cannot be explained with internal conversion process since the expected electron conversion coefficients are 0.33 and 0.11 for the 137 keV and 216 keV transitions, respectively [24]. This is indicative that the decay of band 5 to other structures occurs at 14^- but it is probably fragmented via low energy transitions which cannot be observed. Band 5 consists of intense $M1/E2$ transitions (see table 1) as no $E2$ cross-over transitions have been observed within the band.

3. Discussion

This study is concentrated on the bands in ^{132}Cs which can be understood as a result of the symmetry breaking related to the orientation of the angular momentum vector with respect to the nuclear shape. These are bands 2, 3 and 5.

Band 5 is a regular band (see figure 3) which consists of strong $M1$ transitions. The band is built on the 2636 keV 13^- state, approximately 1.5 MeV above the highest possible two-quasiparticle state which suggests that this is a four-quasiparticle band. The lack of $E2$ cross-over transitions in band 5 clearly shows that this band is built on a weakly deformed structure. In order to better understand the structure of this band we have performed hybrid 3D TAC model calculations [4]. In these calculations the orientation of the total angular

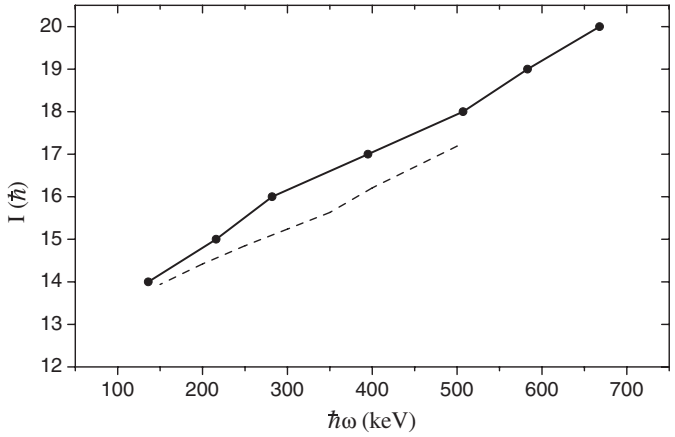

Figure 3. Comparison of experimental spins (solid line, filled circles) with TAC model predictions (dashed line) as a function of rotational frequency.

Table 2. The results from TAC calculations for the $\pi h_{11/2} \otimes \nu[d_{5/2}(h_{11/2})^2]$ configuration in ^{132}Cs. The equilibrium deformation parameters used were $\varepsilon_2 = 0.105$, $\varepsilon_4 = -0.01$ and $\gamma = 34^\circ$. These were obtained as self-consistent values at $\hbar\omega = 150$ keV. For all rotational frequencies the equilibrium tilt angle φ is 0°.

$\hbar\omega$ (keV)	ϑ (deg)	$B(M1, \Delta I = 1)(\mu_N^2)$	$B(E2, \Delta I = 2)(e^2b^2)$
150	33.6	3.634	0.007
200	34.8	3.274	0.005
250	35.7	2.956	0.004
300	36.5	2.675	0.004
350	37.2	2.433	0.003
400	37.9	2.228	0.003
500	40.3	2.003	0.002

momentum with respect to the principal axes of the triaxial core ($\gamma \approx 30^\circ$) is defined by two polar angles ϑ and φ [4], the so-called tilt angles. We used the hybrid TAC model—a version of the TAC model, in which the Nilsson potential is adjusted to be as close as possible to a Woods–Saxon shape. This is achieved, as described in [25], by using the energies of the spherical Woods–Saxon potential plus a deformed part which is an anisotropic harmonic oscillator. It is well known that the Woods–Saxon potential with the universal set of parameters [26] is a better approximation for mass $A \approx 130$ nuclei [27]. The present TAC model calculations are self-consistent with respect to the deformation parameters and the tilt angles. The pairing properties are fixed by the pairing field, which is determined in the TAC model by the gap parameter Δ (for more details see [25]). Since a large reduction of the pairing gap can be expected for multi-quasiparticle excitations in our calculations we used the following gap parameters: $\Delta_\nu = 0.84$ MeV for neutrons and $\Delta_\pi = 0.82$ MeV for protons, which correspond to about 80% of the experimental even–odd mass difference.

The lowest-lying four-quasiparticle negative parity state in ^{132}Cs, according to the calculations, has the $\pi h_{11/2} \otimes \nu[d_{5/2}(h_{11/2})^2]$ configuration at an equilibrium deformation $\varepsilon_2 \approx 0.11, \gamma \approx 34^\circ$. The results from the calculations are summarized in table 2; we were able to follow the $\pi h_{11/2} \otimes \nu[d_{5/2}(h_{11/2})^2]$ configuration up to a rotational frequency $\hbar\omega = 500$ keV where a crossing with other configurations takes place. In figure 3 the

results from the TAC model calculations for the angular momentum versus the rotational frequency are compared with the experimental results. The calculated curve follows well the experimental behaviour although lying about one spin unit below the experimental curve. Such a difference, due to a slightly underestimated moment of inertia, is a known consequence of the absence of quadrupole pairing in the TAC model. On the other hand, the good agreement between the experimental results and the TAC calculations clearly reflects the regularity of the band ($I \propto \hbar\omega$). The TAC calculations predict quite large values for the $B(M1)$ transition probabilities (see table 2) and rather low $B(E2)$ values for the cross-over transitions, which explain the lack of $E2$ transitions within the band. The total angular momentum is generated mainly by the shears mechanism. The tilt angle ϑ (see table 2) is essentially different from 0° and 90° showing that the total angular momentum does not coincide with any of the principal axes, but since the equilibrium tilt angle φ is exactly 0° the total angular momentum is in the plane defined by the short and long axes.

Bands 2 and 3 have been described as chiral partners in [15]. The 3D TAC model calculations [4] have shown that these bands could be associated with an aplanar solution (both tilt angles ϑ and φ are different from 0° and 90°) for the $\pi h_{11/2} \otimes \nu h_{11/2}$ configuration at $\gamma = 36^\circ$ and $\varepsilon_2 = 0.16$. However, due to the moderate quadrupole deformation the chiral structure becomes unstable. The 3D TAC model calculations in [15] have reproduced the experimentally observed energy levels of the chiral partners but failed to reproduce the experimental ratios of reduced transition probabilities $B(M1; I \rightarrow I-1)/B(E2; I \rightarrow I-2)$ in the main chiral partner (band 2). In the present study we have extended the theoretical description of bands 2 and 3 using the core–particle coupling model (CPCM). This is not a self-consistent model but it has a laboratory reference frame basis with the total angular momentum as a good quantum number and restored chiral symmetry. Therefore, it is possible to distinguish between specific properties of the main and the side bands such as reduced transition probabilities.

It is well known that the CPCM and the TAC model are complementary and the use of both simultaneously provides an important advantage over the use of either one of them. A detailed description of the CPCM and the choice of the basis set which is used in the present study can be found in [11]. In the current study the deformation parameters from the 3D TAC calculations were used [15] as input parameters for the CPCM calculations. The quadrupole coupling constant was chosen to be $\chi = 9$ MeV/b^2, a value typical for the region [11]. In the previous implementations of the CPCM [11, 12, 14], only a quadrupole–quadrupole interaction between the valence particles was considered. In the case of ^{132}Cs, it turned out that due to the smaller quadrupole deformation the chiral bands can be described only if a more realistic interaction between the valence particles is included. For this purpose we introduce in the CPCM the surface delta interaction between the valence particles [28]:

$$V_{\pi\nu} = V_l \delta(\vec{r}_\pi - \vec{r}_\nu) + V_s \delta(\vec{r}_\pi - \vec{r}_\nu) \left[\vec{\sigma}(\pi) \bullet \vec{\sigma}(\nu)\right]$$

where π and ν stand for the valence proton and neutron, respectively. In order to reproduce the smooth trend of the energy levels as a function of spin in the present calculations the values of V_l and V_s were attenuated up to 60% of the values proposed in [28]. The matrix element for the $V_{\pi\nu}$ operator between the basis states for the CPCM [11] is given by

$$\langle\psi'|V_{\pi\nu}|\psi\rangle = \delta_{II'}\delta_{KK'}\delta_{RR'}\delta_{rr'}\delta_{LL'}\frac{1}{8\pi}\frac{1}{2L+1}\sqrt{2j_\pi+1}\sqrt{2j_\nu+1}\sqrt{2j_{\pi'}+1}\sqrt{2j_{\nu'}+1}$$
$$\times(-1)^{[(l_\pi+l_\nu)-(l_{\pi'}+l_{\nu'})]/2}(-1)^{j_\pi-j_{\pi'}}\Big[(V_l+V_s)(-1)^{j_\nu-j_{\nu'}}\langle j_\pi s_\pi j_\nu s_\nu|L1\rangle$$

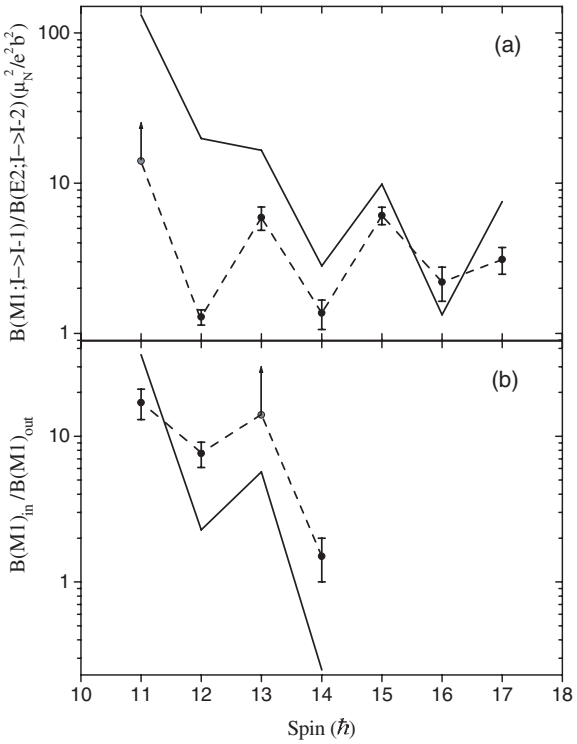

Figure 4. (a) Measured $B(M1; I \to I-1)/B(E2; I \to I-2)$ ratios for band 2 in ^{132}Cs compared to the predictions of CPCM (solid line). (b) Measured $B(M1; I \to I-1)_{\rm in}/B(M1; I \to I-1)_{\rm out}$ ratios for band 3 in ^{132}Cs compared to the predictions of CPCM (solid line). The dashed lines between the experimental points are drawn to guide the eye.

$$\times\langle j_{\pi'} s_{\pi'} j_{\nu'} s_{\nu'}|L1\rangle\frac{1}{2}(1+(-1)^{l_\pi+l_{\pi'}+l_\nu+l_{\nu'}})+(V_l-V_s(1+2(-1)^{l_{\pi'}+l_{\nu'}+L}))$$
$$\times\langle j_\pi s_\pi j_\nu(-s_\nu)|L0\rangle\langle j_{\pi'} s_{\pi'} j_{\nu'}(-s_{\nu'})|L0\rangle\frac{1}{2}((-1)^{l_\pi+l_{\pi'}}+(-1)^{l_\nu+l_{\nu'}})\Bigg].$$

The notation is explained in detail in [11] and follows the standard convention, except for K which stands for the projection of the total angular momentum I on the quantization axis in the laboratory frame.

The CPCM calculations predict that the energy difference between the main and the side band is about 500 keV at spin 10^+ and decreases down to 90 keV at spin 13^+. This is in reasonable agreement with the present results where band 3 (see figure 2) starts at spin 10^+ 447 keV above the main band (band 2) and the smallest energy difference between the levels in bands 2 and 3 is observed at spin 14^+.

The results from the calculations for $B(M1; I \to I-1)/B(E2; I \to I-2)$ ratios in the main partner band and $B(M1; I \to I-1)_{\rm in}/B(M1; I \to I-1)_{\rm out}$ ratios in the side band are presented and compared with experimental values in figure 4. The experimental values were extracted from the experimental γ-ray branching ratios, i.e.,

$$\frac{B(M1; I \to I-1)}{B(E2; I \to I-2)} = 0.697\frac{[E_\gamma(I \to I-2)]^5}{[E_\gamma(I \to I-1)]^3}\frac{T_\gamma(I \to I-1)}{T_\gamma(I \to I-2)}\frac{1}{1+\delta^2}\left(\frac{\mu_N^2}{e^2b^2}\right),$$

and

$$\frac{B(M1;\, I \rightarrow I-1)_{\rm in}}{B(M1;\, I \rightarrow I-1)_{\rm out}} = \left[\frac{E_\gamma(I^{\rm Side} \rightarrow I^{\rm Main}-1)_{\rm out}}{E_\gamma(I^{\rm Side} \rightarrow I^{\rm Side}-1)_{\rm in}}\right]^3 \frac{T_\gamma(I^{\rm Side} \rightarrow I^{\rm Side}-1)_{\rm in}}{T_\gamma(I^{\rm Side} \rightarrow I^{\rm Main}-1)_{\rm out}} \frac{1+\delta^2_{\rm out}}{1+\delta^2_{\rm in}}.$$

We have assumed a pure $M1$ character for the $\Delta I = 1$ transitions (i.e., $\delta = 0$). The last assumption is based on the measured mixing ratios for some of the $M1/E2$ transitions in the chiral bands in ^{128,130,132}Cs [14] which are negligible compared to the uncertainty in branching ratios. The magnitude and the staggering in both $B(M1;\, I \rightarrow I-1)/B(E2;\, I \rightarrow I-2)$ and $B(M1;\, I \rightarrow I-1)_{\rm in}/B(M1;\, I \rightarrow I-1)_{\rm out}$ ratios are well reproduced in the calculations. Moreover, the calculated staggering in the $B(M1;\, I \rightarrow I-1)_{\rm in}/B(M1;\, I \rightarrow I-1)_{\rm out}$ ratios is exactly in phase with the staggering in the $B(M1;\, I \rightarrow I-1)/B(E2;\, I \rightarrow I-2)$ ratios. This characteristic behaviour is a direct consequence from the restrictions imposed on the wavefunctions by the chiral geometry [14] corroborating the chiral interpretation proposed for bands 2 and 3 in [15], namely that these bands occur because the total angular momentum is outside any of the planes defined by the principal axes of the nucleus. The CPCM calculations for ^{132}Cs unambiguously show the important role of the proton–neutron interaction between the valence particles. The good agreement between experiment and theory (see figure 4) can only be achieved if a more realistic interaction than the bare quadrupole–quadrupole interaction is included in the model. We have used the surface-delta interaction [28], but it will be interesting to understand which part of this interaction is particularly responsible for producing the perpendicular coupling of the valence (quasi)particles, a question which requires further experimental information such as absolute transition strengths.

4. Summary

In the present study, we have provided detailed spectroscopic information for the excited bands in doubly odd ^{132}Cs. We have observed a structure which can be understood as a chiral partner of the $\pi h_{11/2} \otimes \nu h_{11/2}$ band and a band built on the $\pi h_{11/2} \otimes \nu[d_{5/2}(h_{11/2})^2]$ weakly deformed configuration which can be understood as a magnetic dipole band. To our knowledge, this is the first case where coexistence of tilted aplanar and tilted planar bands is observed. This interpretation is based on results from the 3D TAC model and it is strongly supported from the experimental data. CPCM calculations have confirmed the previously proposed explanation [15] that in weakly deformed triaxial nuclei, chiral geometry can be achieved due to the residual proton–neutron interaction between the valence particles, which produces the perpendicular coupling between their angular momenta. The same interaction is known to be responsible for the shears mechanisms which generates magnetic dipole bands. This work clearly elucidates the close relation between chiral twin bands and magnetic dipole bands and we hope it will stimulate more detailed theoretical and experimental studies of the residual interaction between the valence protons and neutrons.

Acknowledgments

We wish to thank the staff of IReS for providing the beam and greatly appreciate the technical support in running the EUROBALL IV spectrometer. We gratefully acknowledge helpful discussions with S Frauendorf. This work is supported by the UK EPSRC, the French IN2P3, the US NSF and the EU within TMR contract HPRI-CT-1999-00078.

References

[1] Frauendorf S 2000 *Rev. Mod. Phys.* **73** 463
[2] Frauendorf S 1993 *Nucl. Phys.* A **557** 259c
[3] Baldsiefen G *et al* 1992 *Phys. Lett.* B **275** 252
[4] Dimitrov V I, Frauendorf S and Dönau F 2000 *Phys. Rev. Lett.* **84** 5732
[5] Amita, Jain A K and Sing B 2000 *Atomic Data and Nuclear Data Tables* **74** 283
[6] Koike T, Starosta K, Chiara C J, Fossan D B and LaFosse D R 2001 *Phys. Rev.* C **63** 061304(R)
[7] Petrache C M, Bazzacco D, Lunardi S, Rossi Alvarez C, de Angelis G, de Poli M, Bucurescu D, Ur C A, Semmes P B and Wyss R 1996 *Nucl. Phys.* A **597** 106
[8] Hecht A A *et al* 2001 *Phys. Rev.* C **63** 051302(R)
[9] Hartley D J *et al* 2001 *Phys. Rev.* C **64** 031304(R)
[10] Starosta K *et al* 2001 *Phys. Rev. Lett.* **86** 971
[11] Starosta K, Chiara C J, Fossan D B, Koike T, Kuo T T S, La Fosse D R, Rohozinski S G, Droste Ch, Morek T and Srebrny T 2002 *Phys. Rev.* C **65** 044328
[12] Starosta K, Koike T, Chiara C J, Fossan D B and La Fosse D R 2001 *Nucl. Phys.* A **682** 375c
[13] Bark R A, Baxter A M, Byrne A P, Dracoulis G D, Kibedi T, McGoram T R and Mullins S M 2001 *Nucl. Phys.* A **691** 577
[14] Koike T, Starosta K, Chiara C J, Fossan D B and La Forsse D R 2003 *Phys. Rev.* C **67** 044319
[15] Rainovski G *et al* 2003 *Phys. Rev.* C **68** 024318
[16] Macchiavelli A O, Clark R M, Deleplanque M A, Diamond R M, Fallon P, Lee I Y, Stephens F S and Vetter K 1998 *Phys. Rev.* C **58** R621
[17] Simpson J 1997 *Z. Phys* A **358** 139
[18] Farnea E *et al* 1997 *Nucl. Instrum. Methods Phys. Res.* A **400** 87
[19] Radford D C 1995 *Nucl. Instrum. Methods Phys. Res.* A **361** 297
[20] Krämer-Flecken A, Morek T, Lieder R M, Gast W, Hebbinghaus G, Jäger H M and Urban W 1989 *Nucl. Instrum. Methods Phys. Res.* A **275** 333
[21] Jones P M, Wei L, Beck F A, Butler P A, Byrski T, Duchêne de G, France G, Hannachi F, Jones G D and Kharraja B 1995 *Nucl. Instrum. Methods Phys. Res.* A **362** 556
[22] Hayakawa T *et al* 1997 *Z. Phys.* A **357** 349
[23] Liu Y, Lu J, Ma Y, Zhao G, Zheng H and Zhou S 1998 *Phys. Rev.* C **58** 1849
[24] Hager R S and Seltzer E S 1968 *Nucl. Data Tables* A **4** 1
[25] Dimitrov V I, Dönau F and Frauendorf S 2000 *Phys. Rev.* C **62** 024315
[26] Cwiok S, Dudek J, Nazarewicz W, Nyberg J and Schiffer K 1987 *Comput. Phys. Commun.* **46** 379
[27] Wyss R *et al* 1989 *Nucl. Phys.* A **505** 337
[28] Tajima N 1994 *Nucl. Phys.* A **572** 365